Application of a characterized difference-frequency laser source to carbon monoxide trace detection

Alireza Khorsandi†, Zahra Shabani, Monireh Ranjbar, and S. Ali Hoseinzadeh Salati

Department of Physics, University of Isfahan, 81746-73441 *Isfahan, Iran*

(Received 24 October 2011; revised manuscript received 10 December 2011)

A tunable continuous wave (cw) mid-infrared (MIR) laser based on difference-frequency generation (DFG) in a 1.5-cm long $AgGaS_2$ nonlinear crystal for trace gas detection is reported. Two visible and near-infrared diode lasers were used as pump and signal sources. The MIR-DFG laser was tunable in a wavelength range of 4.75 μm–4.88 μm. The phase-matching (PM) condition was non-critically achieved by adjusting the temperature of the crystal for fixed pairs of input pump and signal wavelengths. The required PM temperatures of the generated MIR-DFG wavelengths have been calculated by using three sets of recent Sellmeier equations and the temperature-dispersion equations of $AgGaS_2$ given by Willer U, *et al.* (Willer U, Blanke T and Schade W 2001 *Appl. Opt.* **40** 5439). Then the calculated PM temperatures are compared with the experimental values. The performance of the MIR-DFG laser is shown by the trace detection of the P(16) carbon monoxide ($^{12}C^{16}O$) absorption line in a laboratory-fabricated absorption cell. The enhanced sensitivity of about 0.6×10^{-4} was obtained through the long path absorption provided by consecutive reflections between coated cylindrical mirrors of a constructed cell.

Keywords: difference-frequency generation, $AgGaS_2$ crystal, multi-pass cell

PACS: 42.62.Fi, 42.65.–k **DOI:** 10.1088/1674-1056/21/6/064213

1. Introduction

Development of coherent laser sources in the mid-infrared (MIR) spectral region is of particular interest for various applications. These include medical and environmental diagnostics as well as security purposes and high resolution inspection of industrial hazardous.[1] In recent years, numerous efforts have been directed toward the generation of many new MIR laser sources offering high sensitivity, selectivity, and fast time responses.[2] They are categorized into two special classes.[3] Distributed-feedback QC (DFB-QC) lasers[4] and all solid states based upon recent developed crystals[5] are classed as class "A". In class "B", nonlinear devices such as difference-frequency generators (DFGs) and optical parametric oscillators (OPOs) cover most of the optical spectrum from visible to far-infrared (FIR) near the newly opened THz domain.[6] Nonetheless, DFG lasers are still very effective in generating narrow linewidth MIR radiation with sufficient tunability and long-time stability. By utilizing new developed nonlinear crystals like GaP and $ZnGeP_2$,[7,8] the DFG laser is a very promising source for emitting a wide range of optical wavelengths. By proper engineering of periodically structured materials quasi-PM can be also possible in many poled crystals such as PPLN and PPKTP.[9] Even though the DFG laser suffers from low conversion efficiency and it is the most complex in design, it is capable of generating high beam quality radiation and further it has minimum susceptibility to environmental disturbances like temperature and pressure. In comparison with the variety of available MIR laser sources, it places DFG laser at the level of highly reliable performance for many years. Numerous continuous wave (cw) and pulsed DFG based MIR sources have been designed and developed for high resolution and quantitative spectroscopy of low molecular and atomic concentrations.[10] The motivation for employing an MIR-DFG laser source is to access the fundamental absorption band of emission species such as CO, NO_x, CH_4, SO_2, and even water vapor, which originate from polluting industries.[11–14] Depending on the gas concentration and the given application, various attractive spectroscopic techniques have been used to detect gaseous species and on-line measurement of the industrial processes both invasively and noninvasively.[15] They are based upon either signal improvement through optical and electrical noise reduction or by using a long optical interaction path length. The latter is inherent to the Beer–Lambert's absorption law where the minimum detectable level

†Corresponding author. E-mail: a.khorsandi@phys.ui.ac.ir

© 2012 Chinese Physical Society and IOP Publishing Ltd

can be improved with the longer optical path lengths provided by multi-pass geometry. The most commonly implemented multi-pass cells have been employed in a countless number of gas sensing devices. They consist of two identical spherical mirrors enclosed in a vacuum housing and separated by a given space which is almost determined by their diameter of curvature.[16,17] The effective optical path length is then limited by the overlapping of laser spots on the mirrors which causes the feature of absorption to be degraded by the signal oscillation. The number of spots can be greatly increased by utilizing non-spherical mirrors and will be spread over the entire mirror surfaces without overlapping the spots. One example is the use of off-axis cylindrical-mirrors providing about 45-m optical path length for a mirror separation of 15 cm.[18] In this investigation, nanoWatt level temperature phase-matched MIR-DFG radiation in the 4.75 μm–4.88 μm region is generated in a 1.5-cm long $AgGaS_2$ nonlinear crystal. The associated phase-matching and acceptance-temperature bandwidth of the generated DFG beam are experimentally measured and compared with the calculated values. Finally, long-time stability of the DFG radiation is also characterized for gaining the mode-hope-free region of its bandwidth tuning in order to access a noise-less scanning width for tracing a carbon monoxide ($^{12}C^{16}O$) absorption line at atmospheric pressure inside an open-path laboratory cell with the detection sensitivity of 0.6×10^{-4}. This is performed by increasing the optical path length through multi reflections of the DFG laser beam between the designed cylindrical mirrors of the cell.

2. MIR-DFG experimental setup

The schematic diagram of the MIR-DFG is shown in Fig. 1. The pump and signal sources of the DFG laser are provided by two cw single mode diode lasers. The pump laser (Opnex HL6738MG) provides an output power of 35 mW operating at a center wavelength of 690 nm and with tuning bandwidth of ±5 nm while the signal source (Sanyo DL-8141-035) had 150-mW output power and tuning bandwidth of ±10 nm around its central wavelength of 808 nm. Their elliptical profiles are slightly modified to the Gaussian shape using anamorphic optics (5AN-3-A-05 Schafter & Kirchhoff) to maintain maximum interaction length inside the nonlinear medium provided by an $AgGaS_2$ uniaxial optical crystal. Accurate measurement of the pump and signal wavelengths is done by a wavemeter (Bristol 821) possessing absolute accuracy of ±0.6 GHz and a repeatability of ±0.06 GHz as provided by the manufacturer. After an anti-reflected polarized beam splitter the residual beams of two pump sources are directed toward a very accurate commercial wavemeter for simultaneous monitoring of their operating wavelengths. The crystal was 1.5-cm long and cut for noncritical 90° phase-matching for e + o → o interaction.

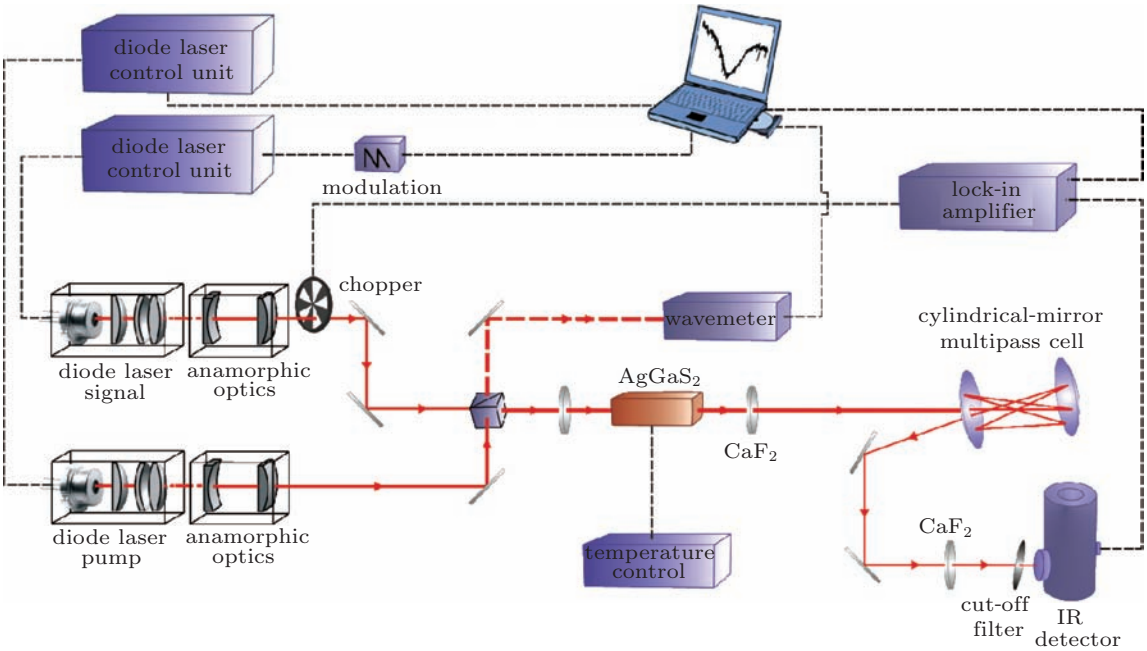


Fig. 1. (colour online) Schematic diagram of the MIR-DFG setup equipped by a cylindrical-mirror multi-pass cell configured for CO gas detection.

The $AgGaS_2$ crystal temperature is controlled by a thermo-electric device (TC200, Thorlabs) within the accuracy of $\Delta T = \pm 0.1$ °C. Therefore, MIR-DFG light can be generated from 4.75 μm to 4.85 μm by proper tuning of the crystal temperature ranging from 29 °C to 100 °C. After passing through a fabricated multi-pass cell, a $f = 15$ cm CaF_2 lens is used to image the spatially Gaussian idler beam on the 1 mm × 1 mm active area of a very fast response MCT N_2-cooled IR detector (MCT 5-010-LN6N, GmbH) possessing average responsivity of about 4500 V/W. In the front, a germanium plate is then used to cut the diode pump beams off.

The amount of electrical and optical noises is then significantly reduced by mechanically chopping the signal diode laser beam and the lock-in technique is used to improve the signal-to-noise ratio (SNR) level of the experiment. The frequency of the chopper was approximately 800 Hz.

3. Output characterization of the generated MIR-DFG radiation

The intensity variation of the generated idler wave with the PM temperature is illustrated in Fig. 2. For carrying out the figure, the pump and signal wavelengths were fixed at 690.048 nm and 804.850 nm, respectively, while the temperature of the crystal is gradually changed around the perfect PM point centered at 75.9 ± 0.1 °C.

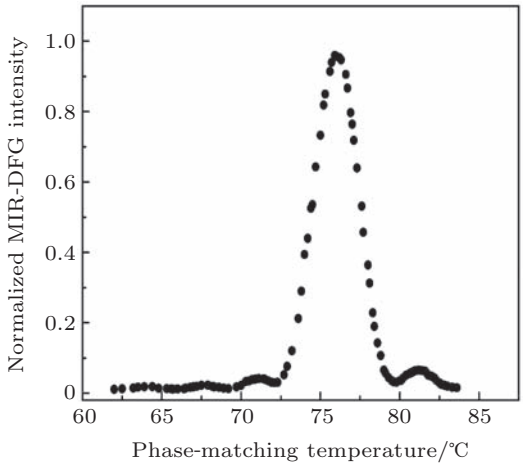


Fig. 2. Intensity variation of the MIR-DFG with the PM temperature of the $AgGaS_2$ crystal. The maximum intensity of the DFG occurred at a temperature of 75.9 °C.

As identified in Fig. 2, next weak harmonics have been clearly occurred in 71.1 °C, 67.9 °C, and 64.4 °C, respectively, which reflect the effective SNR enhancing of the experiment and long-time stability of the DFG beam. As can be deduced from the figure, for gaining the maximum DFG intensity the temperature of the crystal must be controlled within the PM bandwidth of the crystal. It is defined as the DFG intensity decreases to about 40% of its maximum value. Therefore the temperature acceptance bandwidth, $\Delta T_{\rm BW}$, of the crystal is a determinant parameter. From a theoretical point of view, it can be evaluated by expansion of the momentum mismatch, Δk, around perfect PM temperature, $T_{\rm pm}$, as

$$\Delta k = \Delta k_0 + \left.\frac{\partial \Delta k}{\partial T}\right|_{T=T_{\rm PM}} \Delta T_{\rm BW} = \gamma_T \Delta T_{\rm BW}, \quad (1)$$

where

$$\gamma_T = 2\pi \left(\frac{1}{\lambda_{\rm p}} \frac{\partial n_{\rm p}^{\rm e}}{\partial T} - \frac{1}{\lambda_{\rm s}} \frac{\partial n_{\rm s}^{\rm o}}{\partial T} - \frac{1}{\lambda_i} \frac{\partial n_i^{\rm o}}{\partial T} \right) \quad (2)$$

and $\Delta k = \pi / L$ for a given crystal length of L. Therefore by using the temperature-dispersion equations of $AgGaS_2$ crystal given in Ref. [19], and setting the practical pump and signal wavelengths for 690.048 nm and 804.850 nm, respectively, the full width at half maximum (FWHM) of the temperature-acceptance bandwidth can be calculated $\Delta T_{\rm BW} = 4.16$ °C. The correspondence measured value is obtained $\Delta T_{\rm BW} = 4$ °C from Fig. 2, which shows a good agreement with the calculated value.

As given in many literatures and textbooks[20−22] the intensity of the DFG wave is proportional to the linear product of pump and signal intensities. In the case of perfect phase matching, e.g., $\Delta k = 0$, it is

$$I_{\rm DFG} = I_{\rm pump} I_{\rm signal} \eta L, \quad (3)$$

where $I_{\rm DFG/pump/signal}$ are the DFG, pump, and signal intensities, respectively, η is the frequency conversion efficiency and L is the crystal length. The linear dependence of the generated MIR-DFG intensity to the pump and signal power product is shown in Fig. 3, experimentally.

Rapid and high resolution spectroscopy requires a DFG laser with long-time stability and adequate spatial output characteristics. Long time stability of the generated MIR-DFG radiation is shown in Fig. 4.

As clarified in Fig. 4, the MIR-DFG light remains stable in both wavelength and intensity for a relatively long time.

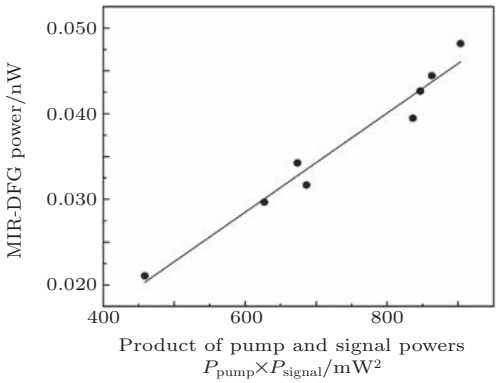


Fig. 3. The DFG intensity versus incident pump and signal powers produced using a 1.5-cm long $AgGaS_2$ crystal. The pump intensity is varied in a specific range while the signal intensity is kept constant. The solid line is the linear fit to the experimental data.

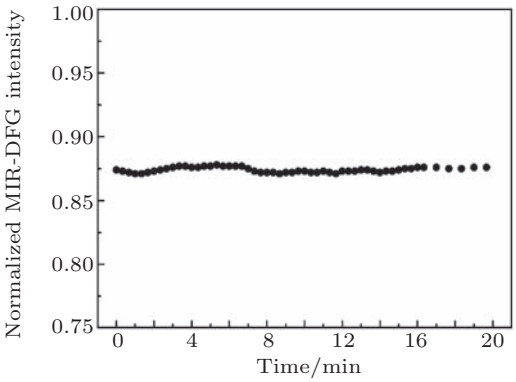


Fig. 4. Variation of the MIR-DFG intensity with time. It is achieved by setting the phase-matching condition for fixed pairs of input pump and signal wavelengths and recording the DFG intensity in 20-s increments. The intensity variation is measured to be about $\Delta I = 0.08\%$ during the measurement.

The main advantage of using non-critical PM, which is investigated in the present work, is to increase the overlap region of interacting waves without walk-off. The amount of ordinary and extraordinary refractive indices $n_{\rm o}$ and $n_{\rm e}$ of the $AgGaS_2$ optical crystal can be changed with the temperature to acquire the PM condition. On the other hand, following the first Sellmeier equation of $AgGaS_2$ crystal in 1971,[23] several sets of Sellmeier and temperature-dispersion equations have been presented in many scientific documents. In Ref. [24] they are completely considered and compared with the measured data. In this article we have employed three sets of those Sellmeier equations and the temperature-dispersion equation given by Takaoka and Kato[19] too, to investigate the agreement between theory and experiment. Starting with the PM calculation from

$$T(^\circ\ \mathrm{C}) = 20 + \frac{\left[n_{\rm e}(\lambda_{\rm p})\lambda_{\rm p}^{-1} - n_{\rm o}(\lambda_{\rm DFG})\lambda_{\rm DFG}^{-1} - n_{\rm o}(\lambda_{\rm s})\lambda_{\rm s}^{-1}\right]}{\left[\dfrac{{\rm d}n_{\rm o}(\lambda_{\rm DFG})}{{\rm d}T}\lambda_{\rm DFG}^{-1} - \dfrac{{\rm d}n_{\rm e}(\lambda_{\rm p})}{{\rm d}T}\lambda_{\rm p}^{-1} + \dfrac{{\rm d}n_{\rm o}(\lambda_{\rm s})}{{\rm d}T}\lambda_{\rm s}^{-1}\right]}, \tag{4}$$

where $\lambda_{\rm DFG/p/s}$ are DFG, pump, and signal wavelengths and ${\rm d}n_{\rm o/e}/{\rm d}T$ is the temperature-dispersions for ordinary and extraordinary waves, respectively. For the pair of practical input pump and signal wavelengths we have generated the possible phase matchable MIR-DFG wavelengths experimentally. Those are compared with the values computed by Eq. (4). The results of this comparison are illustrated in Fig. 5.

To provide Fig. 5, the wavelength of the signal was set on 804.850 nm while the pump wavelength is changed to generate the correspondence MIR-DFG wavelength under the perfect PM condition. As can be followed in Fig. 5, in the lower temperatur region, calculated PM temperatures using the Sellmeier equations reported by Robert referred to Ref. [25], are well suited to the measured values better than 2%. As the temperature is increased above 70 °C, better agreement between the measured PM temperatures and calculated values using Sellmeier equations given by Takaoka and Kato referred to Ref. [19] is obtained. The physical explanation is that at higher temperatures the necessary thermal equilibrium between $AgGaS_2$ crystal and its massive copper housing is a protensive process. Moreover, the temperature gradient is not uniform throughout the length of the crystal.

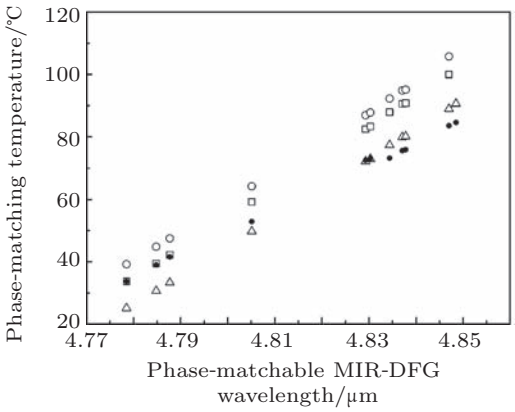


Fig. 5. Measured (•) and calculated PM temperatures for pairs of phase-matchable input pump and signal wavelengths. Three sets of Sellmeier equations; (□) given in Ref. [25], (Δ) given in Ref. [19], and (◯) given in Refs. [26] and [27], have been used in this comparison. The temperature-dispersion equation reported by Takaoka and Kato[19] is used for these sets of Sellmeier equations.

4. Spectroscopic performance

The performance of the characterized MIR-DFG radiation is, firstly, shown as trace detection of the P(16) absorption line of CO molecule in a vacuumed single-pass laboratory cell. It is accomplished by fine tuning of the DFG wavelength over several tens of nanometers at a certain PM temperature. The required mode-hope-free frequency scanning of the MIR-DFG is obtained by using a sawtooth ramp superimposed on the input current of the signal diode-laser source while the frequency of the pump laser was kept constant. The ramp was provided in the LabView environment enabled with about 100-s sample acquisitions in the DFG scanning bandwidth of about 1.1 cm^{-1}. Figure 6 shows the results of the scanning of the MIR-DFG wavelength around the P(16) rotational line of CO centered at 2077.27 cm^{-1} (Ref. [28]) inside a vacuumed 15-cm single-pass cell containing about 43-mbar (1 bar = 10^5 Pa) pure CO (99.99%) gas provided about 60-ppm concentration.

The detection sensitivity of 0.2×10^{-4} is measured by taking into account all the limitations caused by optical elements and electronics. During the measurement, the wavelength of the pump source was fixed at 690.262 nm while the signal is scanned from 805.775 nm to 805.859 nm. The PM is obtained by setting the temperature of the crystal at 65 ± 0.1 °C. DFG wavenumber calibration is performed by accurate measurement of the signal wavelength at the beginning and ending of the ramp by using a commercial wavemeter (Bristol 821).

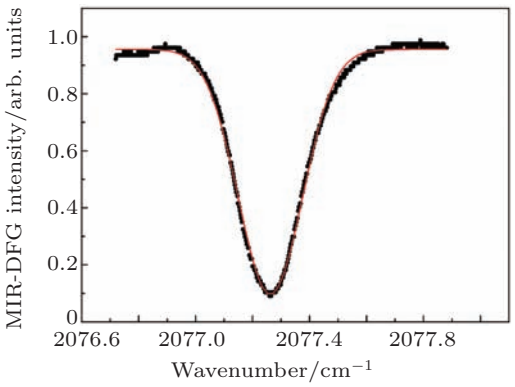


Fig. 6. (colour online) Doppler-broadened absorption spectrum of the P(16) rotational line of a CO molecule centered at 2077.27 cm^{-1} (4.81 μm) in a 15-cm vacuumed single-pass absorption cell at a pressure of 43 mbar. The solid line is the Voigt fit to the experimental data.

To achieve better sensitivity at the same level of DFG output power, an alternative is the lengthening of the absorption path by multi-pass configuration while the physical size remains as compact as possible. Therefore, a multi-pass cell with a physical size of about 30 cm is fabricated and used for the trace detection of CO molecules. It consisted of two off-axis cylindrical mirrors facing each other. By using the ray matrix approach the number and location of the probe beam spots can be determined. The beam pattern and path length can be controlled by rotating the cylindrical mirrors with respect to the optical axis of the device and by adjusting the mirror separation. It was found that under optimum conditions and good alignment the fabricated cell is capable of increasing the optical path length to about 45 m containing 300 round-trip between the mirrors. However, the intensity of the MIR-DFG light imposes a limitation on the number of possible reflections between the mirrors and hence the effective path length. Therefore, owing to the weak DFG intensity, the effective path length is limited to 90 cm after six complete round-trips of the beam inside the cell which translates to effective mirror separation of 15 cm.

In our work, the substrates of two cylindrical mirrors were provided from stainless steel with the radius curvature of about 20 cm. To provide a very smooth and uniform substrate, the mirror surfaces were coated with a thin layer of about 250-nm aluminum. The coating procedure is then completed with another layer of about 500-nm gold to provide minimum loss reflection at the MIR-DFG wavelength in each round trip. The generated MIR-DFG beam is then directed toward a hole on one of the mirrors at an angle of about 30° with respect to the optical axis. After six complete passes between the adjusted mirrors the beam exits through the same hole as indicated in Fig. 1. The residual outgoing DFG beam is then imaged onto the MCT detector.

To evaluate the sensitivity of the newly provided detection system the released smoke from a burned standard cigarette is collected in a voluminous preconcentrator and then flowed toward the pre-vacuumed multi-pass cell. The cigarette smoke contains an amazing array of toxic compounds, such as CO with the concentration of about 0.5% v/v–5% v/v.[29] The direction of the smoke flow was normal to the direction of the beam path inside the cell which ensured that the smoke did not interact with the coating materials and indeed avoid obscurity. The mainstream of the cigarette smoke was then injected to the cell with the flow rate of less than 0.5 lit/min (Ref. [30]) at atmospheric pressure and evacuated at nearly the same rate. The DFG beam is then scanned over the center of the P(16) CO absorption line simultaneously.

The result of this *in-situ* measurement is depicted in Fig. 7.

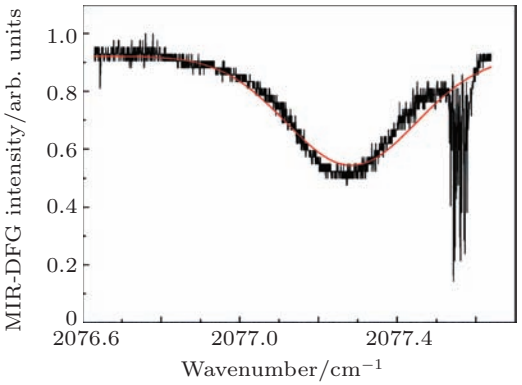


Fig. 7. (colour online) The *in-situ* and sensitive trace detection of the P(16) CO line in the flow of cigarette smoke (0.5 lit/min) after passing six complete reflections inside a cylindrical-mirror multi-pass cell. Measurement is performed at atmospheric pressure and room temperature. The red line is the Voigt fit to the experimental data.

The detection sensitivity is measured 0.6×10^{-4} which has grown three times in comparison with the deduced results shown in Fig. 6. The observed noises imposed on the end of the trace are either due to the signal wavelength fluctuations when it reaches at the ending of the ramp voltage or the electronic noise. The broadening of the traced line is due to the effect of the atmospheric pressure. Whenever the thermal broadening is deconvoluted from the fitted Voigt profile, the concentration of CO molecules can be determined from the homogeneous width of the given lineshape. The Lorentzian width of the traced line given in Fig. 7 is accurately measured by using a commercial PeakFit analyzer while the reference beam was deduced from the trace. As a result a CO concentration of about 7.2% v/v is obtained from the background corrected spectrum, which is comparable with the given value in Ref. [29].

5. Conclusion

We have generated MIR radiation between 4.75 μm–4.88 μm based on difference-frequency generation by using a $AgGaS_2$ uniaxial nonlinear crystal cut for type I 90° noncritical phase-matching condition. The output characterization of the MIR-DFG is demonstrated to be very stable and reliable for an adequate scanning time. The PM temperatures of the DFG wavelengths for the pairs of visible and near-infrared pump and signal wavelengths are calculated by using three different sets of Sellemeier equations and the temperature-dispersion equation given by Takaoka and Kato. The PM temperatures are also experimentally measured and compared with the computed values. This comparison shows that the use of Sellmeier equations reported by Roberts is matched with the measured values at lower PM temperatures while those published by Takaoka and Kato reproduce the experimental PM condition at temperatures higher than 70 °C. The feasibility of the generated MIR-DFG light is shown by trace detection of the P(16) absorption line of CO molecules at 2077.27 cm^{-1} in a 15-cm long single-pass cell containing 60 ppm of CO concentration. A detection sensitivity of about 0.2×10^{-4} is obtained in the provided experimental setup. More sensitive detection is performed through lengthening the optical absorption path by fabricating a multi-pass cell utilizing two off-axis coated cylindrical mirrors. It is shown that at the same level of the DFG laser power, sensitivity is improved to a better value of about 0.6×10^{-4}. The concentration of CO in the condensed cigarette smoke is measured and compared with reported values in the scientific documents. This comparison demonstrates promise for reliable and on-line measurement of toxic gases such as carbon monoxide. As a result, compared with the alternative MIR laser sources, the generated MIR-DFG radiation in combination with the long path spectroscopy technique is still advantageous for sensitive and *in-situ* measurement of emission molecular species.

References

[1] Wondraczek L, Khorsandi A, Willer U, Heide G, Schade W and Heinz Frischat G 2004 *Combust. Flame.* **138** 30

[2] Richter D, Fried A and Weibring P 2009 *Laser & Photon. Rev.* **3** 343

[3] Tittel F K, Richter D and Fried A 2003 *Topics Appl. Phys.* **89** 445

[4] Sharpe S W, Kelly J F, Hartman J S, Gmachl C, Capasso F, Sivco D L, Baillargeon J N and Cho A Y 1998 *Opt. Lett.* **23** 1396

[5] Brandt C, Matrosov V N, Petermann K and Huber G 2011 *Advanced Solid-State Photonics, OSA Technical Digest* (CD), paper AMB15

[6] Petersen E B, Shi W, Chavez-Pirson A, Peyghambarian N and Cooney A T 2011 *Appl. Phys. Lett.* **98** 121119

[7] Jiang Y, Li D, Ding Y J and Zotova I B 2011 *Opt. Lett.* **36** 1608

[8] Shi W, Ding Y J and Schunemann P G 2004 *Opt. Commun.* **233** 183

[9] Ahlawat M, Tehranchi A, Xu C Q and Kashyap R 2011 *Appl. Opt.* **50** E108

[10] Richter D, Fried A, Wert B P, Walega J G and Tittel F K 2002 *Appl. Phys.* B **75** 281

[11] Cao Z S, Gao X M, Deng L H, Chen W D, Yuan Y Q, Zhang W J and Gong Z B 2007 *Spectrochim Acta* Part A: *Mol. Biomol. Spectrosc.* **68** 74
[12] Lancaster D G, Fried A, Wert B, Henry B and Tittel F K 2000 *Appl. Opt.* **39** 4436
[13] Porter J M, Jeffries J B and Hanson R K 2009 *Appl. Phys.* B **97** 215
[14] Wang L, Cao Z, Wang H, Zhao H, Gao W, Yuan Y, Chen W, Zhang W, Wang Y and Gao X 2011 *Opt. Commun.* **284** 358
[15] McCurdy M R, Bakhirkin Y, Wysocki G, Lewicki R and Tittel F K 2007 *J. Breath Res.* **1** R1
[16] Herriott D, Kogelnik H and Kompfner R 1964 *Appl. Opt.* **3** 523
[17] White J U 1942 *J. Opt. Soc. Am.* **32** 285
[18] Kasyutich V l and Martin P A 2007 *Appl. Phys.* B **88** 125
[19] Takaoka E and Kato K 1999 *Appl. Opt.* **38** 4577
[20] Chen W, Boucher D and Tittel F K 2002 *Appl. Phys.* **5** 27
[21] Cao Z, Han L, Liang W, Deng L, Wang H, Xu C, Chen W, Zhang W, Gong Z and Gao X 2008 *Opt. Commun.* **281** 3878
[22] Sutherland R L, McLean D G and Kirkpatrik S 2003 *Handbook of Nonlinear Optics* 2nd edn. (New York: Marcel Dekker Inc.) Chap. 2
[23] Chemla D S, Kupecek P J, Robertson D S and Smith R C 1971 *Opt. Commun.* **3** 29
[24] Willer U, Blanke T and Schade W 2001 *Appl. Opt.* **40** 5439
[25] Roberts D A 1996 *Appl. Opt.* **35** 4677
[26] Harasaki A and Kato K 1997 *Jpn. J. Appl. Phys.* **36** 700
[27] Kato K and Shirahata H 1996 *Jpn. J. Appl. Phys.* **35** 4645
[28] Rothman L S *et al.* 2009 JQSRT **110** 533
[29] Klepeis N E, Ott W R and Repace J L 1999 *J. Exposure Analysis and Environmental Epidemiology* **9** 622
[30] Branton P J, McAdam K G, Winter D B, Liu C, Duke M G and Proctor C J 2011 *Chemistry Central Journal* **5** 1